Polymer Chemistry

ROYAL SOCIETY OF CHEMISTRY

COMMUNICATION

View Article Online
View Journal | View Issue

Cite this: *Polym. Chem.*, 2020, **11**, 1122

Received 12th December 2019,
Accepted 3rd January 2020

DOI: 10.1039/c9py01875a

rsc.li/polymers

Reduced strain mechanochemical activation onset in microstructured materials†

Johanna J. Schwartz, [a,b] Reza Behrou, [c] Bo Cao,[a] Morgan Bassford,[d] Ariana Mendible,[d] Courtney Shaeffer,[d] Andrew J. Boydston *[a,b,e,f] and Nicholas Boechler *[c]

In this study, we show that mechanochemical activation in responsive materials with designed, periodic microstructures can be achieved at lower applied strains than their bulk counterparts. Furthermore, by characterizing two responsive polymeric materials, we have developed a computational model capable of quantitatively predicting mechanochemical activation in geometrically complex structures.

Stimuli responsive materials alter their chemical or physical properties in response to particular environmental cues.[1,2] Exciting examples include polymeric materials that respond to stimuli such as light,[3,4] heat,[5,6] mechanical force,[7,8] electrical potential,[9,10] magnetic fields,[11,12] and pH.[13] A comparatively new class of stimuli-responsive behavior is found in polymer mechanochemistry—the ability to transduce mechanical force along the backbone of a polymer chain to produce a chemical response within the material.[7,8] Generally, the mechanically responsive molecular units (typically referred to as "mechanophores"), which are capable of relieving strain, are placed within the polymer backbone.[7] Mechanophores have been developed to produce a wide range of chemical responses, including effects such as: stiffening or strengthening of materials under stress,[14,15] self-healing,[16–18] small-molecule release,[19–22] rapid depolymerization,[23] catalyst activation,[18,24,25] electrical conductivity changes,[26] and mechanically induced luminescence and color change (mechanochromism).[27,28]

Polymer mechanochemistry is a rapidly growing field, but there are still some significant limitations that hinder its use in practical applications. For solid-state devices, large deformations, often exceeding 100% strain, are typically necessary to achieve activation.[28,29] While large deformations are acceptable in some scenarios, there is a broader and currently unaddressed application base for mechanoresponsive materials that activate at smaller strains.[30,31] Much of the research toward this goal has hitherto focused on a molecular-level, bottom-up approach to improvements in mechanophore activation.[31] To complement chemical-control of mechanochemical activation, we suggest that mesoscopic microstructural geometric tailoring could also be used to enhance mechanochemical activation.

In this study, we show that through the incorporation of strain concentrating features within the context of a periodically "microstructured" material, onset of mechanochemical activation can be tailored to occur at a much lower strain compared to materials lacking judicious geometric design (Fig. 1). We used a calibrated color imaging method to quantify activation within mechanochromic 3D printed and cast materials that leverage a spiropyran mechanophore. In addition, we have developed new numerical models, based on the finite element method (FEM), that are capable of predicting the mechanochemical response in geometrically complex materials. We note that our model is analogous to the model presented by Celestine *et al.*,[32] where the strain and stress fields are directly correlated to the experimentally measured SP activation.[32] We expect that such models will enable the future engineering of mechanochemically active structured materials through topology optimization.

We chose to quantify mechanochromic activation of spiropyran within 3D printed spiropyran-containing polycaprolactone (SP-PCL) and mold-cast polydimethylsiloxane (SP-PDMS) materials. While SP-PDMS materials have been well studied, quantifying the constitutive behavior of thermoplastic elastomers (*e.g.* SP-PCL) is still challenging due to the complex phenomena involved, such as sequential necking under large

[a]*Department of Chemistry, University of Washington, Seattle, WA, 98195, USA. E-mail: aboydston@wisc.edu*
[b]*Department of Chemistry, University of Wisconsin, Madison, WI, 53706, USA*
[c]*Department of Mechanical and Aerospace Engineering, University of California San Diego, La Jolla, CA 92161, USA. E-mail: nboechler@ucsd.edu*
[d]*Department of Mechanical Engineering, University of Washington, Seattle, WA, 98195, USA*
[e]*Department of Chemical and Biological Engineering, University of Wisconsin, Madison, WI 53706, USA*
[f]*Department of Materials Science and Engineering, University of Wisconsin, Madison, WI 53706, USA*

†Electronic supplementary information (ESI) available. See DOI: 10.1039/c9py01875a

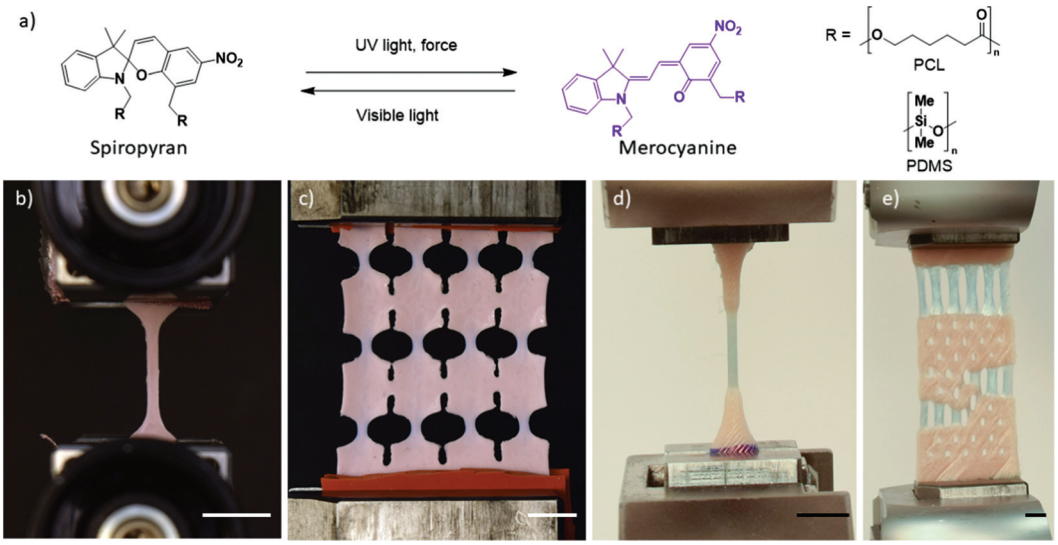

Fig. 1 (a) Generalized depiction of a spiropyran mechanophore activating to become a merocyanine dye. Polycaprolactone (PCL) and polydimethylsiloxane (PDMS) are used in this study. The 'R' symbol denotes attachment points of either PCL or PDMS chains. (b) Spiropyran-containing polydimethylsiloxane (SP-PDMS) dogbone after 50% global strain. (c) SP-PDMS lattice after 50% global strain. (d) Spiropyran-containing polycaprolactone (SP-PCL) dogbone at 50% global strain. (e) SP-PCL lattice at 50% global strain. Scale bars in b–e correspond to 10 mm.

deformation.[33,34] In these materials, two isomeric configurations of merocyanine result in a high-energy blue coloration visible under tension, and a lower-energy purple coloration visible when relaxed after mechanical activation or when activated by UV irradiation.[29]

We used red–green–blue (RGB) image analysis to quantify the mechanochromic activation in our periodically microstructured materials in response to an applied strain.[35,36] For our chosen materials, we defined the range of activation *via* the difference between the blue and green color components, as described in eqn (1):

$$I_{\mathrm{BG}} = 2(\mathrm{B} - \mathrm{G})/(\mathrm{B} + \mathrm{G}). \quad (1)$$

The "averaged" maximum intensity $\overline{I_{\mathrm{BG}}}$, for an applied strain, is obtained by averaging over 100 greatest values of I_{BG} values (pixels) in the measurement domain (see Fig. S8 and S9†). The averaged maximum intesity, $\overline{I_{\mathrm{BG}}}$, was then scaled by analogously averaged maximum intensities obtained for the images of the same sample in several specific states (unloaded, mechanically activated at maximum strain applied, mechanically activated at maximum strain applied and then relaxed, and UV activated). The resulting scaled quantity gives the averaged maximum local activation as follows:

$$A_{\mathrm{actv}} = \frac{\left(\overline{I_{\mathrm{BG}}} - \overline{I_{\mathrm{BG}}}^{\mathrm{ul}}_{\mathrm{max}}\right)\left(\overline{I_{\mathrm{BG}}}^{\mathrm{rx}}_{\mathrm{max}} - \overline{I_{\mathrm{BG}}}^{\mathrm{ul}}_{\mathrm{max}}\right)}{\left(\overline{I_{\mathrm{BG}}}^{\mathrm{UV}}_{\mathrm{max}} - \overline{I_{\mathrm{BG}}}^{\mathrm{ul}}_{\mathrm{max}}\right)\left(\overline{I_{\mathrm{BG}}}^{\mathrm{fn}}_{\mathrm{max}} - \overline{I_{\mathrm{BG}}}^{\mathrm{ul}}_{\mathrm{max}}\right)}, \quad (2)$$

where $\overline{I_{\mathrm{BG}}}^{\mathrm{ul}}_{\mathrm{max}}$, $\overline{I_{\mathrm{BG}}}^{\mathrm{fn}}_{\mathrm{max}}$, $\overline{I_{\mathrm{BG}}}^{\mathrm{rx}}_{\mathrm{max}}$, and $\overline{I_{\mathrm{BG}}}^{\mathrm{UV}}_{\mathrm{max}}$, are the averaged maximum intensities obtained from the images of the same sample in unloaded, mechanically activated at maximum strain applied, mechanically activated at maximum strain applied and then relaxed, and UV activated states, respectively. The UV activated state is interpreted as the maximum possible activation attainable for a given sample. All states were compared for the same elongated sample, to remove effects of thickness variation. Further detail concerning the image processing procedure is given in the ESI.†

We applied our characterization method to study the maximum activation profile as a function of applied uniaxial strain for cast SP-PDMS "bulk" samples in the form of "dogbone" mechanical test specimens (shown in Fig. 1a). The activation response can be seen by the blue markers in Fig. 2c. To target reduced strain onset mechanochromic activation for the case of applied uniaxial "global" strain (change in length between the mechanical tester grips divided by the original length), we introduced strain concentrating elements. Our prediction, within the context of a microstructured material composed of a single constituent material, was that arrays of microstructural elements that are as thin and short as possible, distributed within homogeneous regions that are as mechanically stiff as possible, will trigger reduced strain mechanochromic onset. As such, we cast a SP-PDMS sample in a 3D printed mold, as shown in Fig. 1c and 2a. Comparing Fig. 1b and c, we found that for the same externally applied displacement, the microstructured sample of Fig. 1c shows discernable activation, whereas the bulk sample of Fig. 1b, does not. Quantifying the comparative activation over the tested strain range, we observed a sharp increase in activation of the microstructured sample in comparison with the bulk sample. Quantifying onset of activation as values greater than 6% activation, we found that the microstructured sample reached onset at approximately two times less strain, than the bulk dogbone sample, or approximately 25% *vs.* 50% onset, respectively (see Fig. 2c). Similarly, at approximately 70% strain, we saw experimental activations of ~24% and ~8% for the lattice

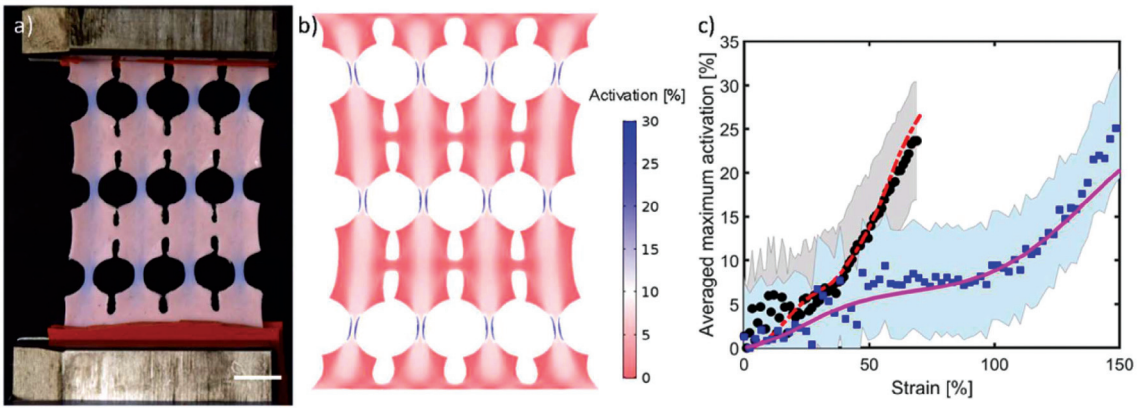

Fig. 2 (a) Experimental image of activation in SP-PDMS lattice at approximately 70% global strain. The scale bar (bottom right) corresponds to 10 mm. (b) Simulation image of activation in SP-PDMS lattice at 70% global strain. (c) SP-PDMS averaged maximum activation *vs.* global strain. The blue square and black circle points correspond to the experimental activation of the dogbone and lattice samples, respectively. The solid and dash-dot lines represent the numerical activation of the dogbone and lattice models. The half-height of the shaded areas represents one standard deviation of the one hundred averaged pixels. The strain for the dogbone simulation is presented in terms of the first strain invariant.

and dogbone, respectively (Fig. 2c). To achieve spiropyran activation of 24% in a bulk dogbone sample, global strains over 145% were necessary.

Similar trends were observed in 3D printed SP-PCL lattices, as can be seen in Fig. 1 and 3. A key difference between the SP-PDMS and SP-PCL systems is that the activation in the SP-PCL system coincides with the onset of plastic deformation, and subsequent "necking" phenomena. After the formation of a neck, the majority of deformation across the sample continues to occur within the necked region. To make clear the implications of the necking phenomenon, we plot the activation measured in the dogbone test specimen as a function of local (defined as the change in length of the necked region over the "original" length of the necked region shortly, where the original state corresponds to a deformed state occurring shortly after necking was observed) and global applied strain, in Fig. 3c and d, respectively. Direct comparison of the two plots can be found in the ESI (see Fig. S9†). As can be seen from the blue dots denoting the activation in the dogbone tests in Fig. 3, the local applied strain definition suggests that extremely large local strains (exceeding ~1500%) are needed to observe activation exceeding 10%. To contrast with the dogbone sample test results, we plot the activation measured as a function of applied global strain in the SP-PCL lattice

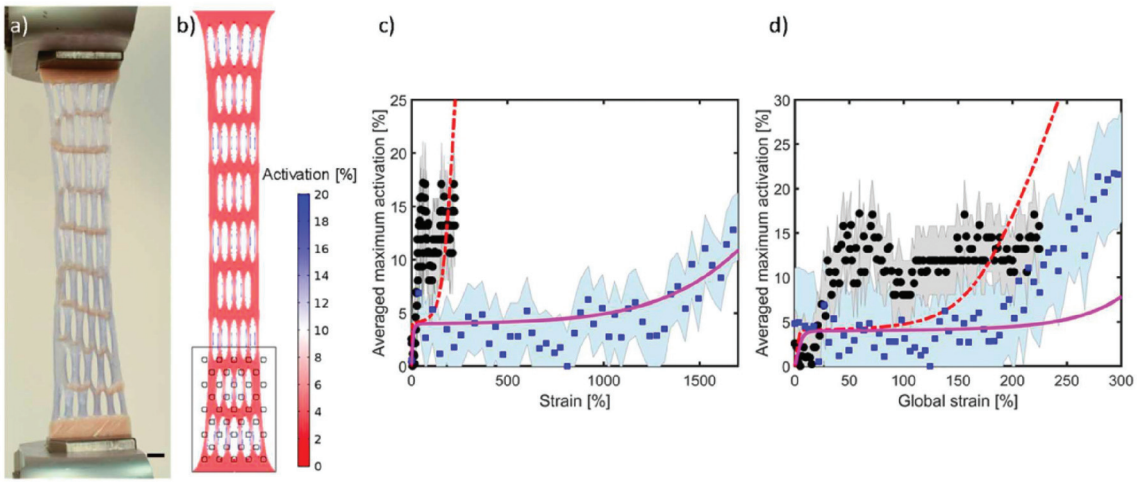

Fig. 3 Experimental image of averaged maximum activation in SP-PCL lattice at approximately 225% global strain. The scale bar (bottom right) corresponds to 10 mm. (b) Simulation of the same lattice at 225% global strain. (c) SP-PCL averaged maximum activation *vs.* strain (local strain for the dogbone and global strain for the lattice). (d) SP-PCL averaged maximum activation *vs.* global strain. The blue square and black circle points correspond to the experimental activation of the dogbone and lattice samples, respectively. The solid and dash-dot lines represent the numerical activation of the dogbone and lattice models. The half-height of the shaded areas represents one standard deviation of the one hundred averaged pixels.

design in both Fig. 3b and d, which is observed to exceed the 10% activation threshold at approximately 30% global applied strain. In both cases the microstructured lattice sample can be seen to pass the 10% activation threshold significantly earlier than the dogbone sample (~8 times and ~50 times lower applied strains, considering the local and global strain description of the dogbone sample activation, respectively). We also note the observation of sequential necking phenomena in the SP-PCL samples, which can be seen in the mechanical testing videos included as part of the ESI.†

For future use in the design and response prediction of microstructured mechanochemically responsive materials, we developed numerical models based on FEM simulations using COMSOL Multiphysics considering geometric and material nonlinearities. For the numerical modeling of SP-PDMS samples, we used a hyperelastic Mooney-Rivlin material model for the material nonlinearity.[33] For the numerical modeling of SP-PCL samples, finite strain elasto-plasticity was considered. The details of material models are provided in the ESI.† Nonlinear curve fitting algorithms were used to extract material properties for the models from the experimentally measured stress–strain curves of the SP-PDMS and SP-PCL dogbone samples.

After matching the mechanical response of the two polymers, we created functions to match the mechanochromic averaged maximum activation intensities as a function of applied uniaxial global strain measured in the dogbone "bulk" samples. The activation profiles were then set as the first principal strain in the case of the SP-PCL and the first strain invariant in the case of the SP-PDMS and implemented as constitutive properties of the two materials in the numerical simulations. Mechanochemical activation of SP has previously been shown to correspond to the first strain invariant in polymeric materials.[37] To mitigate numerical mesh dependency and localization effects in the numerical model, the strain induced local activation is transformed to a smoothed nonlocal activation using a Helmholtz-type differential equation as follows:

$$\bar{A}_{\mathrm{actv}} - \bar{c}_{\mathrm{actv}}\nabla^2\bar{A}_{\mathrm{actv}} = A_{\mathrm{actv}}, \quad (3)$$

where A_{actv} is the local activation, $\bar{A}_{\mathrm{actv}}$ is the smoothed activation, and $\bar{c}_{\mathrm{actv}}$ is the gradient parameter that controls the smoothness of the activation. We note that the minimum value of $\bar{c}_{\mathrm{actv}}$ can be set equal to the local size of the finite element mesh.[38] Here, we set this parameter to 10^{-8}.

The results of modeling of the SP-PDMS and SP-PCL samples are shown in Fig. 2 and 3, respectively. Comparison between the experimentally measured and numerically predicted activation of both the bulk and microstructured lattice materials show good agreement. The one notable exception is that the SP-PCL model does not capture the experimentally observed sequential necking, as can be seen by the simulation of the lattice geometry passing the 10% activation threshold at strains significantly larger than the experiment (Fig. 3c and d). We suggest this is due to the strain being localized to approximately a single row at a time in the experiment, whereas it is distributed in the simulation. Future incorporation of disorder in the model could be a way to decrease the discrepancy and improve accuracy of the numerical prediction.

Conclusions

We have shown that by changing the microstructural geometry of periodic mechanoresponsive polymeric materials, and treating that microstructured material as a new "effective" material, we can achieve activation at much lower overall "global" applied strains. The experimental and numerical results support our hypothesis that the introduction of arrays of microstructural elements that are as thin and short as possible, distributed within homogeneous regions that are as mechanically stiff as possible, will trigger reduced strain mechanochromic onset. However, we note that within the context of a periodic material, decreasingly small and thin inclusions within increasingly larger homogenous regions are expected to create more localized activation within the broader effective material. The ability of microstructure to induce earlier mechanochromic onset has also been shown within in a disordered context in a recent work, wherein cured polymeric microbeads were held together with uncured SP-PDMS bridging material.[39] In this work, a new computational model was also developed that is capable of predicting the activation response in complex mechanochemically responsive materials, which may be useful for future design optimization, including within 3D, additively manufactured structures. The tailored early onset activation shown herein may serve as a means to circumnavigate existing issues with polymer mechanochemistry (*e.g.*, large required strains) and broaden the utility of such materials to lower-strain engineering applications.

Conflicts of interest

There are no conflicts to declare.

Acknowledgements

We thank Bill Kuykendall and the University of Washington MEB user facility, as well as the student technology loan program. We gratefully acknowledge financial support from the Army Research Office (Grant No. W911NF-17–1–0595). A. J. B. acknowledges financial support from the Yamamoto Family, the Office of the Vice Chancellor for Research and Graduate Education at the University of Wisconsin – Madison with funding from the Wisconsin Alumni Research Foundation, and the National Science Foundation (DMR-1452726). This material is based upon work supported by the National Science Foundation Graduate Research Fellowship Program (J. J. S.) under Grant No. DGE-1256082.

References

1 M. Wei, Y. Gao, X. Li and M. J. Serpe, *Polym. Chem.*, 2016, **8**, 127.
2 M. R. Aguilar and J. S. Roman, *Smart Polymers and Their Applications*, Woodhead Publishing, 2014.
3 M. Irie, *Properties and Applications of Photoresponsive Polymers*, 1990.
4 O. Bertrand and J.-F. Gohy, *Polym. Chem.*, 2016, **8**, 52.
5 D. Roy, W. L. A. Brooks and B. S. Sumerlin, *Chem. Soc. Rev.*, 2013, **42**, 7214.
6 Y.-J. Kim and Y. T. Matsunaga, *J. Mater. Chem. B*, 2017, **5**, 4307.
7 J. Li, C. Nagamani and J. S. Moore, *Acc. Chem. Res.*, 2015, **48**, 2181.
8 J. N. Brantley, K. M. Wiggins and C. W. Bielawski, *Polym. Int.*, 2013, **62**, 2.
9 J. Biggs, K. Danielmeier, J. Hitzbleck, J. Krause, T. Kridl, S. Nowak, E. Orselli, X. Quan, D. Schapeler, W. Sutherland and J. Wagner, *Angew. Chem., Int. Ed.*, 2013, **52**, 9409.
10 V. Pillay, T.-S. Tsai, Y. E. Choonara, L. C. du Toit, P. Kumar, G. Modi, D. Naidoo, L. K. Tomar, C. Tyagi and V. M. K. Ndesendo, *J. Biomed. Mater. Res., Part A*, 2014, **102**, 2039.
11 F. Ridi, M. Bonini and P. Baglioni, *Adv. Colloid Interface Sci.*, 2014, **207**, 3.
12 W. Zhang, H. Choi, W. L. Zhang and H. J. Choi, *Polymers*, 2014, **6**, 2803.
13 G. Kocak, C. Tuncer and V. Bütün, *Polym. Chem.*, 2017, **8**, 144.
14 A. L. B. Ramirez, Z. S. Kean, J. A. Orlicki, M. Champhekar, S. M. Elsakr, W. E. Krause and S. L. Craig, *Nat. Chem.*, 2013, **5**, 757.
15 M. B. Gordon, S. Wang, G. A. Knappe, N. J. Wagner, T. H. Epps and C. J. Kloxin, *Polym. Chem.*, 2017, **8**, 6485.
16 H. M. Klukovich, Z. S. Kean, S. T. Iacono and S. L. Craig, *J. Am. Chem. Soc.*, 2011, **133**, 17882.
17 K. Imato, T. Kanehara, S. Nojima, T. Ohishi, Y. Higaki, A. Takahara and H. Otsuka, *Chem. Commun.*, 2016, **52**, 4.
18 R. T. M. Jakobs, S. Ma and R. P. Sijbesma, *ACS Macro Lett.*, 2013, **2**, 613.
19 M. B. Larsen and A. J. Boydston, *J. Am. Chem. Soc.*, 2013, **135**, 8189.
20 B. Cao, N. Boechler and A. J. Boydston, *Polymer*, 2018, **152**, 4.
21 C. E. Diesendruck, B. D. Steinberg, N. Sugai, M. N. Silberstein, N. R. Sottos, S. R. White, P. V. Braun and J. S. Moore, *J. Am. Chem. Soc.*, 2012, **134**, 12446.
22 C. Nagamani, H. Liu and J. S. Moore, *J. Am. Chem. Soc.*, 2016, **138**, 2540.
23 C. E. Diesendruck, G. I. Peterson, H. J. Kulik, J. A. Kaitz, B. D. Mar, P. A. May, S. R. White, T. J. Martínez, A. J. Boydston and J. S. Moore, *Nat. Chem.*, 2014, **6**, 623.
24 A. Piermattei, S. Karthikeyan and R. P. Sijbesma, *Nat. Chem.*, 2009, **1**, 133.
25 P. Michael and W. H. Binder, *Angew. Chem.*, 2015, **127**, 14124.
26 Z. Chen, J. A. M. Mercer, X. Zhu, J. A. H. Romaniuk, R. Pfattner, L. Cegelski, T. J. Martinez, N. Z. Burns and Y. Xia, *Science*, 2017, **357**, 475.
27 Y. Chen and R. P. Sijbesma, *Macromolecules*, 2014, **47**, 3797.
28 G. R. Gossweiler, G. B. Hewage, G. Soriano, Q. Wang, G. W. Welshofer, X. Zhao and S. L. Craig, *ACS Macro Lett.*, 2014, **3**, 216.
29 G. I. Peterson, M. B. Larsen, M. A. Ganter, D. W. Storti and A. J. Boydston, *ACS Appl. Mater. Interfaces*, 2015, **7**, 577.
30 M. H. Barbee, K. Mondal, J. Z. Deng, V. Bharambe, T. V. Neumann, J. J. Adams, N. Boechler, M. D. Dickey and S. L. Craig, *ACS Appl. Mater. Interfaces*, 2018, **10**, 29918.
31 H. Oka, K. Imato, T. Sato, T. Ohishi, R. Goseki and H. Otsuka, *ACS Macro Lett.*, 2016, **5**, 1124.
32 A. D. N. Celestine, N. R. Sottos and S. R. White, *Strain*, 2019, **55**, 3.
33 T. K. Kim, J. K. Kim and O. C. Jeong, *Microelectron. Eng.*, 2011, **88**, 1982.
34 H. Cho, S. Mayer, E. Pöselt, M. Susoff, P. J. in 't Veld, G. C. Rutledge and M. C. Boyce, *Polymer*, 2017, **128**, 87.
35 D. A. Davis, A. Hamilton, J. Yang, L. D. Cremar, D. Van Gough, S. L. Potisek, M. T. Ong, P. V. Braun, T. J. Martínez, S. R. White, J. S. Moore and N. R. Sottos, *Nature*, 2009, **459**, 68.
36 H. Zhang, Y. Chen, Y. Lin, X. Fang, Y. Xu, Y. Ruan and W. Weng, *Macromolecules*, 2014, **47**, 6783.
37 Q. Wang, G. R. Gossweiler, S. L. Craig and X. Zhao, *J. Mech. Phys. Solids*, 2015, **82**, 320.
38 C. Giry, F. Dufour and J. Mazars, *Int. J. Solids Struct.*, 2011, **48**, 3431.
39 R. C. Rohde, A. Basu, L. B. Okello, M. H. Barbee, Y. Zhang, O. D. Velev, A. Nelson and S. L. Craig, *Polym. Chem.*, 2019, **10**, 5985.